Chemical Activation of Single-Walled Carbon Nanotubes for Hydrogen Adsorption

Milton R. Smith, Jr.,[‡] Edward W. Bittner,[‡] Wei Shi,[†,‡] J. Karl Johnson,[†,‡] and Bradley C. Bockrath*[,‡]

National Energy Technology Laboratory, U.S. Department of Energy, P.O. Box 10940, Pittsburgh, Pennsylvania 15236, and Department of Chemical and Petroleum Engineering, University of Pittsburgh, Pittsburgh, Pennsylvania 15261

Received: December 5, 2002; In Final Form: February 12, 2003

Adsorption isotherms for hydrogen on single-walled nanotubes (SWNTs) subjected to various types of pretreatment have been measured by a tapered-element oscillating mass analyzer. Isotherms at room temperature over a range of pressures up to 48 bar have been measured. We demonstrate that activation of the SWNT samples by mild oxidation in CO_2, followed by heat treatment in an inert atmosphere, increases the hydrogen adsorption capacity of the SWNT samples by about a factor of 3 at 48 bar. Computer simulations have been performed to model the adsorption isotherms. Bundles of homogeneous (all the same diameter) and heterogeneous (composed of a number of different diameters) nanotubes have been considered. Isotherms computed using a standard graphitic potential for the nanotubes give remarkably good agreement with the experimentally measured isotherms before activation with CO_2. The effect of activation is modeled by independently increasing the nanotube spacing and the solid−fluid interaction potential. We find that nanotube spacing alone cannot account for the measured increase in adsorption capacity. Increasing the interaction potential gives isotherms that are qualitatively different from experiments, while a combination of increased nanotube spacing and increased solid−fluid potential gives rough agreement with experiments.

I. Introduction

The unique porosity of single-walled carbon nanotubes (SWNTs) has prompted considerable interest in their gas-adsorption properties. The present need for better materials for hydrogen storage has led to much of the interest in this direction. Several reviews of this rapidly growing area have appeared.[1−3] Among the various reports are claims that significant amounts of hydrogen are taken up by SWNTs. Claims of high values of hydrogen adsorption have been made in reports of investigations at low temperature,[4] room temperature,[5,6] and even higher temperatures.[7] In contrast, most theoretical calculations of hydrogen adsorption have given considerably lower estimates.[8−18] These results may indicate that physisorption on pure nanotubes may not be an effective method of storing hydrogen. Other experimental studies have found very limited uptake of hydrogen,[19−21] in agreement with simulations. However, variations in the experiments may be due to differences in the way the SWNT samples were prepared or pretreated.

Chemical activation is one option for improving adsorption characteristics. Although it has a long history of application in carbon chemistry, its potential for use with the recently synthesized carbon nano-structures is just beginning to become evident.[22,23] It has been shown that Xe adsorption on SWNTs is dramatically affected by the pretreatment procedure.[24] Eklund and co-workers have shown that the hydrogen uptake on nanotubes at low temperatures can be increased radically by activation of the nanotube samples.[23]

In the work described below, we have used a tapered element oscillating mass analyzer (TEOM) to obtain isotherms for hydrogen adsorption on SWNTs at 25 °C over the range of pressure from one to 48 bar. This instrumental method is based on measurement of the weight change observed as a function of the applied hydrogen pressure in a flow-through system. The application of this instrument to determine adsorption isotherms has been recently demonstrated in the case of light alkanes (methane−butane) on silicalite.[25] In the work reported below, samples of SWNTs were used as-received and after various pretreatments. The most remarkable results were obtained using a simple activation procedure based on partial oxidation using carbon dioxide at 600 °C. The adsorption of excess hydrogen increased markedly after SWNTs were activated by this procedure. Activated samples were found to adsorb 1.2 wt % hydrogen at 48 bar and 25 °C. Details of the activation procedure are described in a recent paper.[26] Characterization of the surfaces of the same raw and purified nanotubes as used in this work has been made by a pulse adsorption technique using the TEOM.[27]

We also present molecular simulations as a means of identifying possible reasons for the observed increase in adsorption in the samples that have been activated by CO_2 oxidation. Theoretical calculations of hydrogen adsorption on SWNTs have been performed using various methods.[8−18] With few exceptions, these studies indicate only modest uptake of hydrogen at room temperature and moderate pressures. Ab initio simulations that indicate the potential for higher uptake are subject to substantial error because the description of the H_2−nanotube interaction within the tight-binding or density functional approximations is not expected to be accurate for physisorption.[28−32]

All of the theoretical studies performed so far have been carried out on SWNT samples that are, by necessity, idealized

* Corresponding author. E-mail: bockrath@netl.doe.gov.
† University of Pittsburgh.
‡ National Energy Technology Laboratory, U.S. Department of Energy.

10.1021/jp027631v CCC: $25.00
Published on Web 04/01/2003

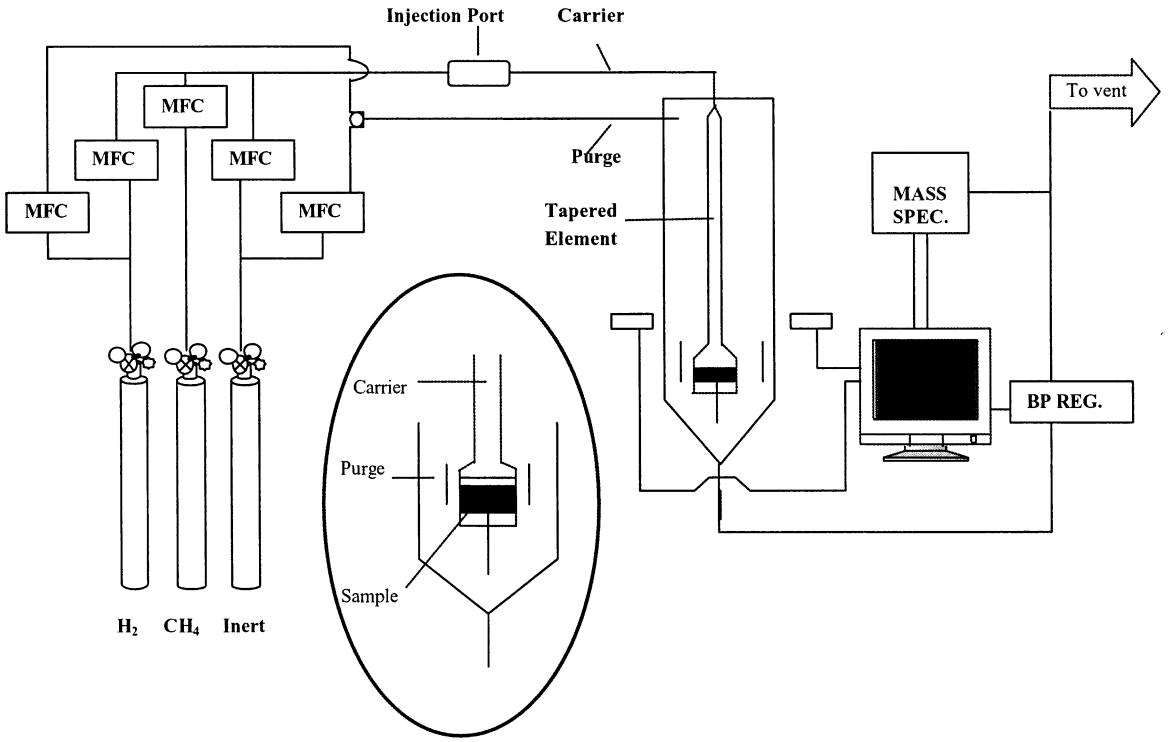

Figure 1. Block diagram of the Rupprecht and Patashnick TEOM 1500 and associated hardware.

in some ways. Some of the studies consider only single isolated nanotubes. Other studies assume idealized nanotube bundles composed of perfect hexagonal or square arrays of identical nanotubes, all of the same diameter and chirality. In reality, experimentally produced SWNT bundles are composed of nanotubes of different diameters and chiralities.[33−37] While nanotubes pack into a hexagonal array, the packing is not expected to be perfect because of the distribution of nanotube diameters in a bundle. At least some nanotube samples have a significant number of defects that may contain carbonyl or other oxygenated groups.[38] Nanotube bundles are also not perfectly straight. There is curvature over length scales of hundreds of nanometers, allowing nanotube bundles to cross one another, leading to complex secondary structures. The external surfaces of the SWNT bundles are also complicated by the presence of amorphous carbon and catalytic metals. All of these factors make exact modeling of real SWNT bundles a very difficult task. In addition, the exact form of the nanotube−hydrogen potential is unknown and could only be computed accurately from very high-level electronic structure methods that include electron correlation (e.g., coupled cluster or configuration interaction); such calculations are impractical for SWNTs because of the large number of atoms involved. It is also not known exactly how the presence of defects changes the interaction potential. Activation processes, such as the one used in this study to improve hydrogen uptake, further complicate the description of the nanotube samples by adding unknown chemical and topological changes to the underlying structure. Previous simulations have accounted for defects in an approximate way by including point dipoles or point charges.[39] Size heterogeneity in different bundles has been modeled by picking nanotube diameters randomly from a given size distribution.[40] In this study we examine the effect of the nanotube diameter distribution and packing on hydrogen uptake. We also vary the nanotube−hydrogen interaction potential by arbitrarily increasing the potential well depth to mimic the effect of chemical activation.

II. Experimental Methods

A block diagram of the experimental apparatus including the TEOM Series 1500 Pulse Mass Analyzer (Rupprecht and Patashnick Co.) is given in Figure 1. The TEOM Series 1500 is a flow-through microbalance that detects mass changes by an inertial system. It was initially used to study coke deposition on zeolite catalysts,[41] and has since found general application for following mass changes in a variety of chemical systems including a recent study of the adsorption isotherms of light hydrocarbons on zeolites.[25] It employs a tapered glass element to measure mass changes. The element consists of a hollow glass tube that leads the gas stream through a cylindrical sample bed, diameter 4 mm, height 6 mm, located at its lower end. Samples were packed into the bed between "Astro quartz" wool plugs and retained there by a ventilated, gold-plated metal cap. Gas streams were controlled using a manifold that included mass flow controllers and a back-pressure regulator. Instrument control and data recording were managed through a PC. The control system allowed the programmed selection of the gases, their flow rates, system pressure and temperature, and other functions. Two gas streams were supplied to the instrument; one passes through the sample in the packed bed (reactive gas) and the other sweeps the volume outside the sample bed (purge gas). The tapered-element was enclosed within a heated stainless steel pressure vessel. The instrument is capable of operating from ambient temperature to 700 °C and from ambient pressure to 48 bar. The combined flow of both gas streams is sampled at the exit port by a capillary tube that serves as a transfer line to a quadrupole mass spectrometer.

The operating principle of the instrument is based on the relationship between changes in the mass of the sample bed to

changes in the frequency of oscillation of the tapered element. The element is stimulated to vibrate at its natural frequency by a mechanical system. The frequency of oscillation is measured by an optical system through two ports in the pressure vessel. Mass changes are determined by the following equation:

$$\Delta m = \frac{k}{\frac{1}{f_1^2} - \frac{1}{f_2^2}} \tag{1}$$

where f_1 and f_2 represent the frequencies observed at two different loadings, and k is an empirically determined constant. The instrument was equilibrated at the isotherm temperature and flow conditions in order to determine the value of k. The frequency of the empty reactor was measured without the retaining cap in place; then the procedure was repeated with the cap in place. The constant was calculated using the known mass of the cap.

The mass changes observed in the instrument as the pressure is varied result from both changes in density of the free gas within the oscillating element and the change in the amount of gas adsorbed by the sample. To obtain the isotherm of the excess adsorbed gas, the amount due to the change in density of the free gas must be subtracted from the total. The values due to the free gas density changes were obtained from experiments with the reactor empty. In this case, the observed mass change increased in a nearly linear fashion with pressure. Measurements were then taken with a sample in place under exactly the same conditions. Isotherms were generated by subtracting the mass change found with the empty reactor from the corresponding value found with the packed reactor for each step in pressure. A correction was applied to the empty reactor data to account for the volume occupied by the sample (see calculations below).

In a typical experiment, a sample of 30−50 mg was packed into the bed between 20 and 40 mg of quartz wool used as plugs. The bed was flushed with dry helium or nitrogen, then heated to 200 °C for at least 2 h. After the signal from the mass spectrometer indicated that the release of small amounts of water and oxygen was complete, the sample was cooled to 25 °C and both reactant and purge gases were switched to hydrogen at a flow rate from 10 to 50 cm^3/min. Hydrogen was used as both purge and reactant gas in all experiments reported here to eliminate possible instrumental artifacts that may arise due to back-mixing of a dissimilar purge gas into the packed bed.

The pressure program was only begun after all of the inert gas had been swept from the reactor by hydrogen as indicated by the response of the mass spectrometer sampling the exit stream. Then the pressure was taken from ambient to 48 bar in seven steps. It was held constant for 10−20 min after each increment. At the end of the ascending program the pressure was returned to ambient using 1.4 bar decrements to avoid expelling the sample from the bed. The entire program was then repeated several times. Note that in these experiments, the origin of the pressure/mass change data is ambient pressure. Thus, isotherms refer to the increment in hydrogen adsorption above that already taken up at one atmosphere.

As noted above, a correction was applied to account for the portion of the free gas volume in the packed bed that is occupied by the sample and quartz wool. The correction was made by multiplying the mass changes for the empty reactor by the ratio of the free volume for the packed to that of the empty reactor. The total free volume sensed by the oscillating element was determined by applying the ideal gas law to the variation of the measured mass of the empty reactor when the hydrogen pressure was increased from ambient to 48 bar. The error in the specific volume from assuming ideal gas behavior at 48 bar and room temperature is about 3%. The volume of the sample was calculated from the mass of carbon in the sample and the theoretical density. The correction factor found using these values had a relatively small effect on the calculated amount of adsorbed hydrogen because the measured free volume of the reactor element is roughly an order of magnitude larger than the volume occupied by the sample. The mass change assigned to excess hydrogen was expressed as weight percent of gas adsorbed based on the total mass of carbon in the sample. The latter was determined by thermal gravimetric analysis (TGA). Atomic adsorption spectroscopy was used to verify the identity of the residual catalytic metals recovered after the TGA analysis.

The weight percent of excess H_2 adsorbed is given by

$$\text{wt \%} = 100\frac{\Delta m_s - V_{corr}\Delta m_E}{f_c m_{ads} - \Delta m_{ads}} \tag{2}$$

where Δm_s is the mass change for the packed bed after changing to pressure P_i, V_{corr} is the volume correction factor (∼0.977) to account for the volume occupied by the sample, Δm_E is the corresponding mass change in the empty reactor on reaching P_i, f_c is the fraction of SWNT sample that is carbon, m_{ads} is the mass of the SWNT sample, and Δm_{ads} is the weight lost after pyrolysis at either 200 or 700 °C.

The values used for each mass change were averages of from 80 to 160 data points taken over the 10−20 min interval after a plateau was reached following each pressure step. Points in the isotherms are averages of 2−13 individual determinations of excess hydrogen for each pressure. The most extensively measured sample was calculated from 7 cycles of pressure up and down made over 12 days. Data were taken from the 20 min plateaus at each step of the seven programs up in pressure and the 10 min plateaus of six programs down. The last depressurization failed and was not included. Sample standard deviations for the average of the 13 values for each point in the isotherm were between 0.03 and 0.11 wt %, being smaller at lower pressures. No trends were apparent over time nor differences noted for pressurizing or depressurizing sequences. One set of values for wt % H_2 (reaching 1.54 wt % at 48 bar) was tested for rejection using updated values for Dixon's Q test. The resulting $Q_{EXP} = 0.72$ indicated rejection at the 99% confidence interval and this set was therefore not incorporated in the isotherm in Figure 6. The remaining set of 12 values for each pressure has standard deviations between 0.02 and 0.03 wt % for each point.

Nanotubes were purchased from Tubes@Rice in two grades. "Raw Material Grade" was obtained as a solid, fibrous mat. It was subjected to light grinding to make it easier to load into the sample cell. Grinding was performed by agitation for 4−8 min in a small agate ball mill (Wiggle Bug, Brinkman Instruments). "Purified Grade" was purchased as a suspension in toluene. Typically 10−15 mL of the suspension was withdrawn from the bulk sample and evaporated in a stream of dry nitrogen at ambient temperature. When toluene was no longer evident, the sample was further dried at 140 °C for up to a week. Activated nanotubes were prepared by partial oxidation in a tube furnace held at 600 °C using a stream of CO_2 and argon at about a 50/50 ratio. Details are given in another paper.[26] A sample of activated carbon (G-32 H, 4 × 10 mesh, Süd Chemie Inc.) was used to compare with the nanotube samples. The hydrogen, nitrogen, and carbon dioxide isotherms

of this sample have been determined independently at this laboratory by a volumetric technique.[42] Hydrogen was "Extra Dry" grade (>99.9%) from Matheson Tri-Gas. Helium and nitrogen were Matheson Tri-Gas UHP grade. The gases were further dried by passage through a Matheson Gas Purifier Cartridge Type 452 (4A molecular sieve).

III. Simulation Methods

Adsorption isotherms were computed from grand canonical Monte Carlo (GCMC) simulations.[43] The Silvera-Goldman potential[44] was used to describe the H_2-H_2 interactions. This potential has been shown to be accurate for computing equilibrium bulk properties over a very wide range of temperatures and pressures.[45] The H_2−nanotube interaction was taken as a pairwise summation over H_2-C interactions computed from the Crowell-Brown potential.[46] This type of potential has been shown to reproduce experimental H_2−graphite adsorption isotherms and isosteric heats at low temperatures.[47] The solid-fluid potential used in the simulations is actually an integrated potential form so that a single polynomial function was fitted to the H_2−exohedral (outside) nanotube interactions and a second polynomial was used for the H_2-endohedral (inside) nanotube interactions. Thus, each type of nanotube was described by two polynomial functions.[9] We have constructed several different types of SWNT bundles in order to study the effects of diameter heterogeneity and packing effects on hydrogen uptake. We have constructed bundles by choosing nanotubes of various diameters from a given diameter distribution to mimic experimental distributions.[36] We have also developed bundles based on an arbitrary diameter distribution for comparison with results from the experimental distributions. The bundles were packed by placing the first nanotube in the bundle at the center of the cell. The next nanotube was placed at a random position far enough away so as to ensure no overlap with the existing nanotube. The nanotube was then brought in a straight line toward the center of the box until the van der Waals (vdW) gap between the first and second nanotubes achieved some pre-specified value. The vdW gap is defined as the shortest distance between the walls of adjacent nanotubes, as measured from atom-center to atom-center. Subsequent nanotubes were added in a fashion similar to the second, except that the tube is brought in until its vdW gap with any other tube in the bundle reaches the specified value. The simulation box is a rectangular parallelepiped with a height (z-direction) of 34 Å and equal x and y dimensions. Periodic boundary conditions were applied in all three directions. The x and y dimensions were large enough to eliminate nearest neighbor interactions with tubes or hydrogen in the periodic images in order to mimic isolated SWNT bundles. Typical values of the width of the simulations box were between 100 and 250 Å, depending on the size of the bundle. A sample nanotube bundle is shown in Figure 3. The bundle contains 45 nanotubes and corresponds to bundle type a in Table 1.

Typical GCMC moves[43] were attempted randomly with probabilities of 0.4 for displacements and 0.3 each for creation and deletion. The systems were first equilibrated for 5×10^6 steps, followed by 10^7 steps for data collection. Adsorption isotherms were computed for five different classes of nanotube bundles shown in Table 1. The bundles contain from 20 to 100 nanotubes. Samples a−c are constructed to mimic two different diameter distributions observed in the experiment.[36] Samples d and e were constructed from an arbitrary diameter distribution. Samples b and c have almost the same diameter distribution. Sample c contains half as many nanotubes as sample b. Samples d and e have exactly the same diameter distribution, with sample e having 2.5 times as many nanotubes as sample b.

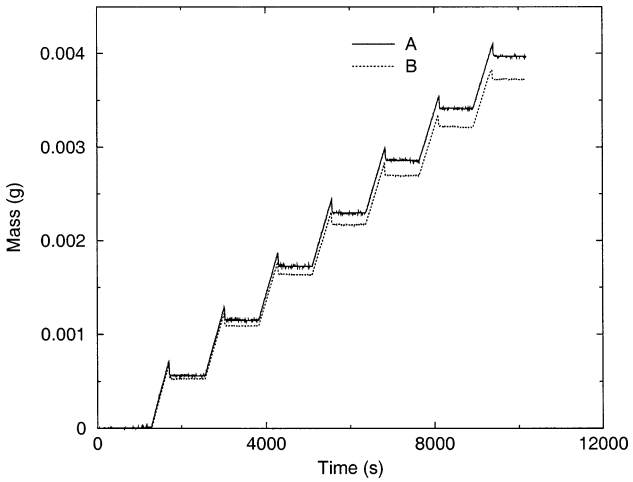

Figure 2. Mass vs time as the H_2 pressure increases in steps of about 7 bar from one to 48 bar. Curve A is a 29 mg sample of purified Rice nanotubes after CO_2 oxidation and B is for the empty reactor.

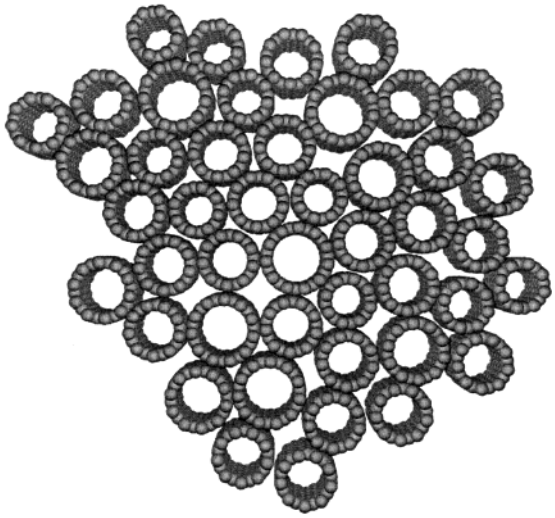

Figure 3. Sample nanotube bundle used in the molecular simulation. This bundle contains 45 nanotubes with diameters drawn randomly from a distribution similar to that observed in experiments (sample a in Table 1).

From two to 10 different realizations of each bundle were constructed by starting the construction procedure outlined above with different random number seeds. Adsorption isotherms were computed for each of the realizations and the averages were reported. The differences in adsorption on different bundle realizations for a specified diameter distribution were typically on the order of the uncertainties in the simulations. To be consistent with the experiment, the excess adsorption is calculated as

$$\text{wt \%} = 100\,\frac{(N_{H_2,P} - N^{rep}_{H_2,P}) - (N_{H_2,1} - N^{rep}_{H_2,1})}{6N_C} \qquad (3)$$

where $N_{H_2,P}$ is the number of adsorbed H_2 molecules in the simulation cell at pressure P, $N^{rep}_{H_2,P}$ is the number of H_2 molecules at pressure P in the cell when the attractive part of the potential between H_2 and nanotube is turned off, $N_{H_2,1}$ and $N^{rep}_{H_2,1}$ are the corresponding values at the reference pressure, i.e., 1 atm, N_C is the number of carbon atoms in the simulation cell. The excess adsorption defined in eq 3 is directly comparable

TABLE 1: Classes of Nanotube Bundles Studied in the Molecular Simulations in This Work

bundle ID	number of tubes	(8,8)	(9,9)	(10,10)	(11,11)	(12,12)	average diameter (Å)
a	45	10	25	5	5	0	12.35
b	100	6	29	35	28	2	13.44
c	50	3	14	18	14	1	13.45
d	20	0	4	14	2	0	13.42
e	50	0	10	35	5	0	13.42

to that from the experiment defined in eq 2. Note that this definition of the excess adsorption is different from that typically used because of the reference to one atmosphere rather than to vacuum.

IV. Results and Discussion

Figure 2 contains the mass data used as a basis for the hydrogen isotherms described below. Curve A is the record of the mass changes for the packed reactor, and curve B is that for the empty reactor. Both mass curves closely follow the pressure curves (not shown). The initial spike found at the leading edge of each pressure step is due to an overrun of the set point by the back-pressure regulator. The mass change curve for the packed reactor reaches a new plateau after each pressure change and remains constant. This behavior is consistent with a physisorption process without a significant kinetic barrier. Separate experiments were made to test whether slow adsorption might take place over time scales much longer than the 20 min intervals used here. No measurable mass changes were found even when the initially formed plateau was extended for 28 h at 48 bar. A very similar pattern was found for the depressurization data. These results for the kinetics of hydrogen adsorption and those reported on a different set of SWNTs of somewhat larger diameter[5] are distinctly different. In the later case, 6 h was required for the pressure to equilibrate during the volumetric measurement made at room temperature, indicative of a significant kinetic barrier. No such barrier was found in any of the adsorption results given here.

The adsorption isotherm for hydrogen on an activated carbon is given in Figure 4 curve A. The isotherm is nearly linear up to the limit of pressure for these measurements, reaching a value of 0.66 wt % at 48 bar. Isotherms for hydrogen and other gases up to about 19 bar have recently been determined by a volumetric technique on this same lot of activated carbon.[42] Comparison of the two sets of data reveals the value measured volumetrically at room temperature and 14 bar is 1.2 mol/kg, while the corresponding point from the TEOM at 25 °C is 1.04 mol/kg. There is reasonable agreement between the values obtained by the two different techniques. Note that the TEOM and volumetric methods have different reference points. The TEOM technique measures the increment in hydrogen adsorbed above 1 atm (see eq 2), while the volumetric technique begins the measurement of excess adsorption after the sample chamber has been evacuated. Given that the amount adsorbed at 1 atm is only about 0.01 wt %, the observed differences between the TEOM and the volumetric method cannot be attributed to the difference in reference points.

Two isotherms for a sample of "Raw Material" SWNTs from Rice are also shown in Figure 4. Curve B was taken after the sample had been heated in situ to 200 °C under a flow of helium, then cooled before the isotherm experiment was begun. Curve C was obtained in a subsequent experiment after the sample had been heated in a similar manner but to 700 °C. Pyrolysis at 700 °C reduced the affinity of the sample for hydrogen by a significant amount. (The apparently anomalous value at 41 bar for curve C was due to the influence of one of only two values determined under these conditions for this sample.)

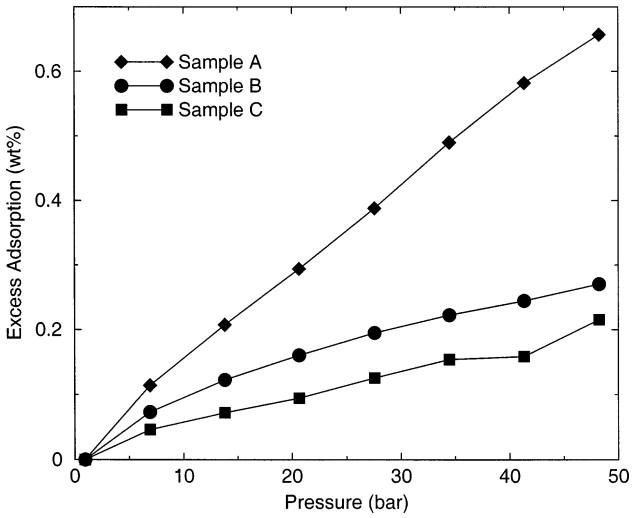

Figure 4. Hydrogen isotherms for activated carbon (A) and "Raw Material" as-produced Rice nanotubes after treatment at 200 °C (B) and 700 °C (C) in flowing helium. The lines are drawn to guide the eye.

Evidence that the pyrolysis of the raw material resulted in considerable loss of functional groups was provided by the in-line mass spectrometer used to monitor the exit gases throughout the course of heating to 700 °C. Hydrogen, methane, and carbon oxides were detected as the temperature increased. After the sample had returned to 25 °C, the TEOM measured a weight loss of 13.2 mg, or 23.2% of the sample weight. Data in Figure 4 are based on total mass of nonmetals and have been corrected for loss of mass to allow direct comparison of the samples.

In comparison to the sample of activated carbon (curve A), the "Raw Material" nanotube samples have at best roughly one-half the storage capacity under the same pressure. Again, the saturation loading of either the fresh or the pyrolyzed samples has not been reached at the highest pressure used here, although curve B seems to show some curvature not apparent in curve A.

Adsorption isotherms on "Purified" nanotubes obtained from Tubes@Rice are shown in Figure 5. These tubes have undergone oxidation by reflux in 2.6 M nitric acid for 12 h.[36] The oxidation is reported to selectively remove amorphous carbon, leaving behind a greater proportion of nanotubes in the sample.[36] The samples were represented as containing greater than 90% SWNT. The relative amount of the residual metal catalyst left in the sample increases as well. Presumably an overlay of graphitic carbon protects these particles from removal by oxidation. The metal content of the sample used here was determined by complete combustion using TGA in combination with atomic adsorption spectroscopy of residual oxides. The metals content was 8.8 wt % and the spectroscopy confirmed the presence of nickel and cobalt. The isotherms given in Figure 5 were normalized on the basis of total carbon content to obtain a more useful comparison, but were not adjusted for the fraction purported to be SWNT.

Isotherms A and B in Figure 5 were taken sequentially using the same protocol as employed for raw material above. To a first approximation, the amounts of hydrogen adsorbed by the purified nanotubes and the raw material are similar. This result is contrary to the simple expectation that the purified material should adsorb a greater amount of hydrogen per sample weight because of its higher nanotube content. Heating to 700 °C in

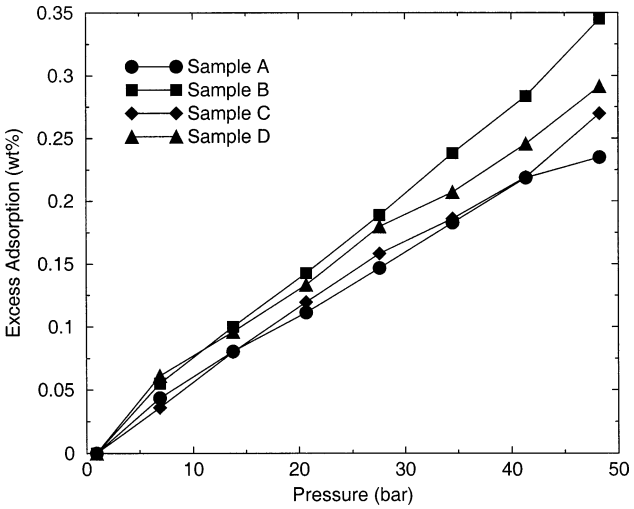

Figure 5. Comparison of adsorption isotherms of hydrogen on "Purified" Rice tubes: Sample A was heated at 200 °C in He. Sample B is sample A heated at 700 °C in He. Sample C is sample B after removal and milling in air. Sample D is sample C treated at 700 °C in H_2. The lines are drawn to guide the eye.

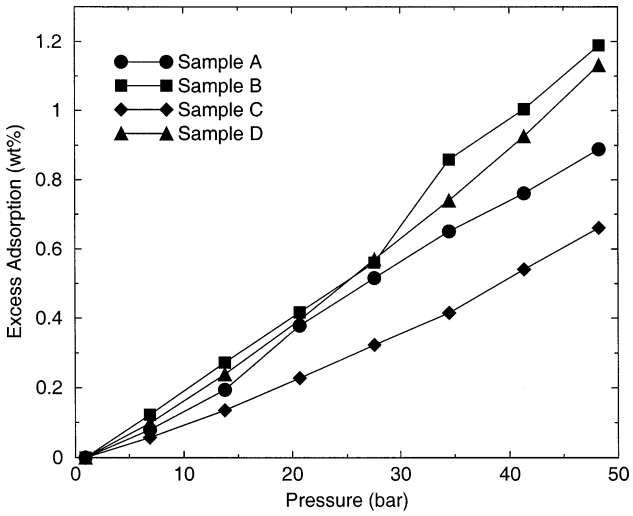

Figure 6. Adsorption isotherms for hydrogen on "Raw Material" Rice SWNTs after CO_2 oxidation (sample A). Sample B is derived from A after heating at 700 °C in H_2. Sample C consists of "Purified" Rice nanotubes after CO_2 oxidation. Sample D is sample C after heating at 700 °C in He. The lines are drawn to guide the eye.

flowing He led to a modest increase in hydrogen adsorption as shown by comparing curves A and B. Perhaps it is more significant that the slope over this nearly linear region of the isotherm has increased after pyrolysis. Thus, the difference between the two may well increase at hydrogen pressures above those used here.

The mass spectra of the gases produced during pyrolysis were similar to those seen with the raw material and consistent with the loss of carboxyl and other oxygen-containing functionalities. The mass loss following pyrolysis was 12.7% and may be compared with the value of 23.2 wt % found with the raw material. The functional groups responsible for this weight loss were likely introduced during the oxidative purification with nitric acid. Further evidence of their connection to the adsorption properties of the SWNTs was provided by a separate experiment in which another sample was carried through five cycles of pyrolysis at 700 °C over several days. The isotherms found before and after the first pyrolysis are nearly identical to A and B given in Figure 5. However, repetition of the initial pyrolysis had little further effect on the storage capacity or the slope of the isotherms. The relative amounts of the products from pyrolysis detected by the mass spectrometer were much reduced after the first cycle. Thus, the sample is chemically stable to 700 °C after the first pyrolysis cycle and no evidence for further annealing of the physical structure is found in the isotherms.

As mentioned in the Experimental section, these nanotube samples are difficult to pack into a small bed because their fibrous nature resists compaction. A mild mechanical milling procedure renders them much more amenable to packing. To determine whether this procedure has an effect on the adsorption properties, the sample was removed after isotherm B in Figure 5 was completed, milled by agitation in a small ball mill, and repacked in the bed. Milling the sample in air in this way decreased its adsorption capacity slightly (curve C). This loss was mostly restored (curve D) when the sample was again pyrolyzed, this time in flowing H_2. Thus, the effects seem more related to the oxidative consequences of milling in air rather than the milling itself. Mild ball milling in air introduces oxygen-containing functional groups into the nanotubes as evident from the evolution of CO and CO_2 observed in the mass spectrum on heating to 700 °C. In view of the small change, the issue was not pursued further.

Activation of the nanotube samples took place in two steps. The first step was conducted by partial oxidation of a roughly 200 mg sample of nanotubes in a tube furnace under a stream of CO_2 at about 600 °C. Burn-out during the initial oxidative procedure removed about 37 wt % of the purified nanotube sample. In the case of the raw material, about 21% of the weight was removed during CO_2 oxidation. TEM images taken before and after the reaction with CO_2 show that in the case of the purified-grade material the rope-like structures are left intact.[26] It is unexpected that a larger fraction of the purified sample would oxidize in the CO_2 treatment than for the raw material. This may be a result of the damage done to the nanotubes during the purification procedure.[48]

A marked improvement in the amount of hydrogen adsorbed was obtained for both the raw material and the purified tubes (Figure 6, curves A and C) after the first step. The amount adsorbed at 48 bar has increased from 0.29 to 0.89 wt % for the raw material and from 0.23 to 0.64 wt % for the purified material. The second step of activation was accomplished in the TEOM by heating the oxidized tubes to 700 °C in a flow of He or H_2. This induced further weight loss. For example, the oxidized raw material lost an additional 20% when pyrolyzed under H_2 at 700 °C. The pyrolysis led to a further increase in hydrogen adsorption. The cumulative effect of the two steps is a significant increase in hydrogen storage capacity (Figure 6, curves B and D). Values of 1.16 wt % ("Purified") and 1.2 wt % ("Raw Material") were reached at 48 bar.

The data in hand do not permit an assignment of hydrogen adsorption capacity to particular fractions of carbon such as those identified by TGA, for example. Thus, if the material removed by CO_2 oxidation had been relatively inert toward hydrogen adsorption, the remaining material would show a corresponding increase in percent adsorption. Removal of this dilution effect could account for increases of 16% for the raw material and 59% for the purified material, but that is far short of the more than 3-fold increase actually found. Instead, the large magnitude of the increase points toward a form of chemical activation.

It is reasonable to assume that this activation for adsorption may occur by opening the internal surfaces of tubular structures by oxidative destruction of part of the tube wall. In fact, evidence has been presented for thinning and opening of multiwalled

tubes by partial oxidation with CO_2 at 850 °C, a somewhat higher temperature than used here.[22] The potential benefit created by removing tube end-caps and thus enhancing gas storage properties through the use of this method has been claimed in a patent, although no adsorption data were given.[49] Another study has demonstrated that opening the sidewalls of SWNTs by a combined cycle of oxidation and pyrolysis enhances the kinetics of xenon adsorption.[39] In this case, oxidation was accomplished with ozone, and the pyrolytic removal of the carboxylic groups so created was performed at the same temperature as used here, 700 °C. The maximum in the observed rate of xenon adsorption was found after a considerable percentage of the carbon had been etched away.

Parallels exist with the result reported here. The activation by CO_2 is likewise an oxidation. Because it is carried out at 600 °C it is simultaneously a pyrolysis, thus combining the oxidation/pyrolysis cycle in one step. It also removes a considerable fraction of the carbon in the sample. The adsorption isotherms measure a thermodynamic property, and we are unable to detect evidence for kinetic limitations in any case. However, TPD experiments described in the xenon adsorption work show that the majority of the sites that are more accessible after oxidation also desorb xenon at higher temperatures, implying deeper potential wells.[39] On the other hand, comparison of our data with computer simulation results (see below) indicate that in this case the increase in adsorption cannot be ascribed to opening of entry ports to the nanotubes alone.

It should be noted that pyrolysis of purified tubes results in a modest increase in hydrogen storage (Figure 5), but in the case of "Raw Material" SWNTs it results in a decrease of smaller magnitude (Figure 4). This result is puzzling, but we note that in the first case an oxidation using nitric acid was done to generate purified material before the pyrolysis was carried out. In the later case, pyrolysis was applied without prior oxidation. Annealing of the rope-like structures of nanotubes at elevated temperatures has been reported and must be considered as another potential side effect of pyrolysis. Annealing may reduce the amount of interstitial volume in bundles of the raw material. The differences seen in Figure 4 are rather small, and would be in concert with the expectation that the relative amount of hydrogen taken up in the interstitial spaces is a small part of the total. Thus, the contradictory trends in adsorption may be the result of the dominance of an annealing effect in the case of raw nanotubes and the opening of additional porosity in the case of the purified nanotubes.

V. Simulation Results

We have computed H_2 adsorption isotherms on each of the nanotube bundles listed in Table 1. The isotherms on the different bundles are in quantitative agreement with one another. This is an important result because it indicates that the simulation results are not strongly dependent on the details of the bundle geometry or even the nanotube size distribution within the bundle. This insensitivity to the details of the geometry was unexpected.

The excess adsorption isotherms are plotted in Figure 7. Results from simulations on bundle samples b, c, and e from Table 1 are plotted along with experimental data for purified nanotubes before being subjected to CO_2 oxidation (curve B from Figure 5). Adsorption isotherms from simulations on other bundles are very similar and are not shown for the sake of clarity. The agreement between the simulation and experimental isotherms is striking. Assuming that the solid−fluid interaction potential is accurate, the remarkable agreement between simulations and experiments indicates that the samples before CO_2 oxidation can be considered to be mainly composed of nanotube bundles (once the weight of the metal has been subtracted) and that amorphous carbon present in the sample and pore-blocking functional groups do not severely inhibit hydrogen adsorption. On the other hand, it could be that the assumed H_2−nanotube interaction potential is too weak and that the adsorption is attenuated in the experiment due to pore blocking or unopened nanotubes to a degree that gives fortuitous agreement with simulations. Given the insensitivity of the computed adsorption isotherms to the bundle size and nanotube diameter distribution, we cannot deduce anything about the experimental nanotube bundle geometry from the agreement between the simulations and experiments.

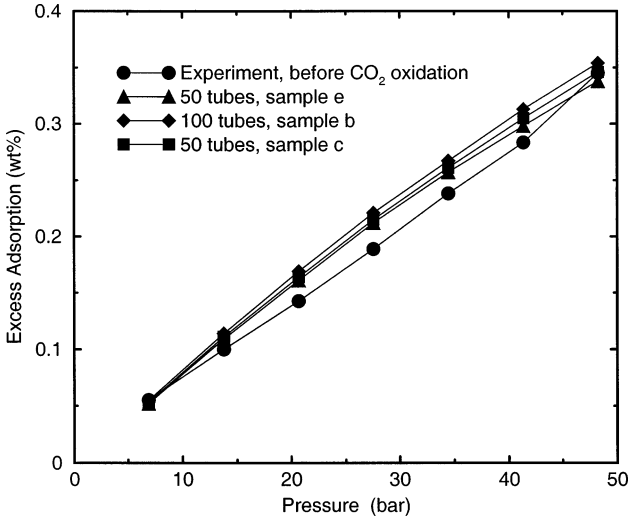

Figure 7. Adsorption isotherms computed from simulations for several of the bundles listed in Table 1. The experimental data for a sample of purified nanotubles heat treated to 700 °C, (sample B from Figure 5) are shown for comparison. The lines are drawn to guide the eye.

We next examine the possible causes for the dramatic increase in adsorption observed after CO_2 oxidation and subsequent heat treatment. The oxidation treatment will likely etch holes in the nanotubes and deposit oxygen-containing functional groups at these defect sites. We therefore hypothesize that the increase in adsorption capacity may be due to an enhancement of the solid−fluid potential (as a result of the introduction of polar functional groups), or due to an increase in the available volume (from holes etched in the tubes), or to a combination of these. We test this hypothesis by arbitrarily increasing the gap between the nanotubes, or increasing the strength of the solid−fluid potential, or a combination of both increasing the gap and the strength of the interaction potential. This procedure is only a first-order approach to modeling the effects of CO_2 oxidation. Simulations of nanotubes with side-wall holes and explicit functional groups will be part of a future study. The optimal vdW gap for a perfect SWNT array is about 6.4 Å for maximizing the excess volume adsorbed at moderate pressures.[9] This is double the experimentally measured gap in as-produced nanotube bundles. Our simulations (not shown) indicate that increasing the vdW gap alone is not sufficient to reproduce the magnitude of the increase in adsorption observed after CO_2 oxidation and subsequent heat treatment of the nanotube samples. The solid-fluid potential V_{sf} was increased by simply multiplying the potential by an arbitrary factor. Thus, 1.5 V_{sf} means that the potential has been increased by 50%. Isotherms computed from bundles with various values of the vdW gap and V_{sf} multipliers are shown in Figure 8. The experimental data for H_2 adsorption on the CO_2 oxidized and heat treated

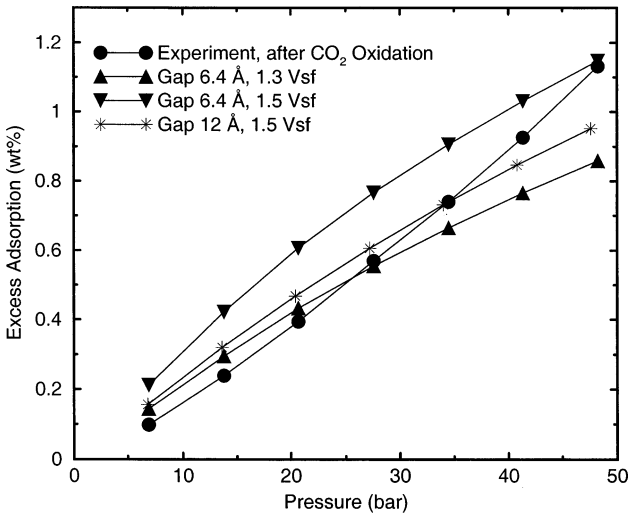

Figure 8. Adsorption isotherms computed from simulations with increased gap spacing and enhanced solid−fluid attractive potentials. All the simulations are for bundles containing 45 nanotubes with a diameter distribution given by sample a, from Table 1. Experimental data from Figure 6 sample D are shown as circles. The up triangles denote the results for a bundle with the vdW gap increased to 6.4 Å and the solid−fluid potential increased by 30%. The down triangles represent data for a bundle with a vdW gap of 6.4 Å and the potential increased by 50%. The stars are for a vdW gap of 12 Å and a potential increased by 50%. The lines are drawn to guide the eye.

purified nanotubes (sample D from Figure 6) are plotted as circles in Figure 8. Simulations show that increasing the interaction potential while holding the vdW gap fixed at 3.2 Å produces a curve that is substantially concave downward and hence cannot match both the low- and high-pressure regions of the experimental data, which are approximately linear in pressure. This indicates that the mechanism for increasing the adsorption in experiments cannot be described by a simple increase in the solid−fluid potential. An adsorption isotherm on a bundle with a vdW gap of 6.4 Å and a potential of 1.3 V_{sf} is represented by the up triangles in Figure 8. These simulation data agree well with the experiments at low pressures but underpredict the amount adsorbed at high pressures. If a potential of 1.5 V_{sf} is used with a gap of 6.4 Å (down triangles), then the simulations and experiments agree at high pressure but not at low pressure. If we increase the vdW gap further, the curvature of the simulation data decreases. The simulations for a vdW gap of 12 Å and 1.5 V_{sf} are shown as stars in Figure 8. This value of the vdW gap is unrealistically large and yet still gives an isotherm that is slightly concave downward. This indicates that no physically reasonable values of the vdW gap and interaction potential can be found that can accurately reproduce the shape of the experimental isotherms observed on samples that have been oxidized with CO_2. The simulated isotherms are all curved and tend to approach a plateau region at higher pressures, while the experimental isotherms are all approximately linear or concave upward in coverage at all pressures studied. However, reasonable qualitative agreement between experiments and simulations is achieved for 1.5 V_{sf} and a vdW of 12 Å. All of the isotherms shown in Figure 8 were computed from nanotube bundles of type a from Table 1. Calculations for nanotube bundles from sample b are similar to those shown for sample a and are not shown for clarity.

VI. Conclusions

The hydrogen adsorption properties of SWNTs have been investigated using a TEOM to determine mass changes on exposure of the samples of up to 48 bar pressure. The rates of adsorption and desorption are apparently fast and indicative of physisorption. The isotherms are still ascending at the upper pressure limit of the instrument and it is clear that the saturation loading of these materials is not defined by these experiments. The raw and purified SWNTs samples do not adsorb as much hydrogen as a typical sample of activated carbon under similar conditions. Most importantly, we have shown that a simple, controlled oxidation with CO_2 activates SWNTs for adsorption of hydrogen. A roughly 3-fold increase in the amount of hydrogen adsorbed is observed at the highest pressures. Up to 1.2 wt % hydrogen was observed in the best case. Molecular simulations have been performed to compute the adsorption isotherms of hydrogen on finite size nanotube bundles that are composed of nanotubes of various diameters. The size of the bundles studied ranged from 20 to 100 tubes drawn from three different diameter distributions. Adsorption isotherms from simulations on the various bundles are all in relatively good agreement with one another. The amount of hydrogen adsorbed at these conditions does not appear to be a strong function of the size of the bundle or the diameter distribution for the samples studied here. Remarkably good agreement is seen between the simulations and experimental isotherms on nanotube samples before activation. This implies that the solid−fluid potential for the nanotubes before activation is fairly accurate and that the endohedral sites are available for adsorption on these samples. It is also possible that the agreement between simulations and experiments is fortuitous and that the unactivated samples do not adsorb H_2 inside the nanotubes, although this scenario seems unlikely. Adsorption isotherms on nanotube bundles with larger free volumes and stronger solid−fluid attractive potentials were computed to evaluate whether these factors could explain the observed increase in H_2 uptake capacity after activation. It was found that a bundle with a vdW gap of 12 Å and a potential increased by 50% agrees fairly well with the experimental data, although the shape of the simulated and experimental isotherms differs. Given that the size of the vdW gap and the increase in the potential are both too large to be physically reasonable, we conclude that the increase in adsorption upon activation is not solely due to increased free volume and solid−fluid potential enhancement. Hence, standard physisorption potentials do not adequately describe the activated nanotube samples. However, chemisorption cannot make a significant contribution to the experimental isotherms because the process is completely reversible and adsorption and desorption kinetics are too fast to be described by chemisorption.

This work shows that activation of SWNT samples can profoundly impact the adsorption of H_2. Understanding the process will ultimately help optimize the activation, further enhancing the adsorption capacity.

Acknowledgment. M.R.S. served as a National Research Council Senior Associate at NETL. J.K.J. and E.W.B. are Oak Ridge Institute for Science and Education Faculty Research Associates at NETL. W.S. was supported under the University Partnership Program at NETL. Reference in this work to any specific commercial product is to facilitate understanding and does not necessarily imply endorsement by the United States Department of Energy.

References and Notes

(1) Dresselhaus, M. S.; Williams, K. A.; Eklund, P. C. *MRS Bull.* **1999**, *November*, 45−50.
(2) Dillon, A.; Heben, M. J. *Appl. Phys. A* **2001**, *72*, 133−142.
(3) Cheng, H. M.; Yang, Q. H.; Liu, C. *Carbon* **2001**, *39*, 1447−1454.

(4) Ye, Y.; Ahn, C. C.; Witham, C.; Fultz, B.; Liu, J.; Rinzler, A. G.; Colbert, D.; Smith, K. A.; Smalley, R. E. *Appl. Phys. Lett.* **1999**, *74*, 2307−2309.
(5) Liu, C.; Fan, Y. Y.; Liu, M.; Chong, H. T.; Cheng, H. M.; Dresselhaus, M. S. *Science* **1999**, *286*, 1127−1129.
(6) Dillon, A. C.; Jones, K.; Bekkedahl, T. A.; Kiang, C. H.; Bethune, D. S.; Heben, M. J. *Nature* **1997**, *386*, 377−379.
(7) Chen, P.; Wu, X. B.; Lin, J.; Tan, K. L. *Science* **1999**, *285*, 91−93.
(8) Wang, Q.; Johnson, J. K. *J. Chem. Phys.* **1999**, *110*, 577−586.
(9) Wang, Q. Y.; Johnson, J. K. *J. Phys. Chem. B* **1999**, *103*, 4809−4813.
(10) Williams, K. A.; Eklund, P. C. *Chem. Phys. Lett.* **2000**, *320*, 352−358.
(11) Darkrim, F.; Levesque, D. *J. Phys. Chem. B* **2000**, *104*, 6773−6776.
(12) Gordon, P.; Saeger, P. B. *Ind. Eng. Chem. Res.* **1999**, *38*, 4647−4655.
(13) Stan, G.; Cole, M. W. *J. Low Temp. Phys.* **1998**, *110*, 539−544.
(14) Rzepka, M.; Lamp, P.; de la Casa-Lillo, M. A. *J. Phys. Chem. B* **1998**, *102*, 10894−10898.
(15) Darkrim, F.; Levesque, D. *J. Chem. Phys.* **1998**, *109*, 4981.
(16) Simonyan, V. V.; Diep, P.; Johnson, J. K. *J. Chem. Phys.* **1999**, *111*, 9778−9783.
(17) Lee, S. M.; Lee, Y. H. *Appl. Phys. Lett.* **2000**, *76*, 2877−2879.
(18) Simonyan, V. V.; Johnson, J. K. *J. Alloys Compd.* **2002**, *330−332*, 659−665.
(19) Yang, R. T. *Carbon* **2000**, *38*, 623−626.
(20) Tibbetts, G. G.; Meisner, G. P.; Olk, C. H. *Carbon* **2001**, *39*, 2291−2301.
(21) Pinkerton, P. E.; Wicke, B. G.; Olk, C. H.; Tibbetts, G. G.; Meisner, G. P.; Meyer, M. S.; Herbst, J. F. *J. Phys. Chem. B* **2000**, *104*, 9460−9467.
(22) Tsang, S. C.; Chen, Y. K.; Harris, P. J. F.; Green, M. L. H. *Nature* **1994**, *372*, 159−162.
(23) Pradhan, B. K.; Harutyunyan, A. R.; Stojkovic, D.; Grossman, J. C.; Zhang, P.; Cole, M.; Crespi, V.; Goto, H.; Fujiwara, J.; Eklund, P. C. *J. Mater. Res.* **2002**, *17*, 2209−2216.
(24) Kuznetsova, A.; Mawhinney, D. B.; Naumenko, V.; Yates,J. T., Jr.; Liu, J.; Smalley, R. E. *Chem. Phys. Lett.* **2000**, *321*, 292−296.
(25) Zhu, W.; van de Graaf, J. M.; van de Broeke, L. J. P.; Kapteijn, F.; Moulijn, J. A. *Ind. Eng. Chem. Res.* **1998**, *37*, 1934−1942.
(26) Smith, M. R., Jr.; Hedges, S. W.; LaCount, R.; Kern, D.; Shah, N.; Huffman, G.; Bockrath, B. *Carbon*, in press.
(27) Bittner, E. W.; Smith, M. R., Jr.; Bockrath, B. C. *Carbon*, in press.
(28) van Mourik, T.; Gdanitz, R. J. *J. Chem. Phys.* **2002**, *116*, 9620−9623.
(29) Rappé, A. K.; Bernstein, E. R. *J. Phys. Chem. A* **2000**, *104*, 6117−6128.
(30) Misquitta, A. J.; Szalewicz, K. *Chem. Phys. Lett.* **2002**, *357*, 301−306.
(31) Wu, X.; Vargas, M. C.; Nayak, S.; Lotrich, V.; Scoles, G. *J. Chem. Phys.* **2001**, *115*, 8748−8757.
(32) Milet, A.; Korona, T.; Moszynski, R.; Kochanski, E. *J. Chem. Phys.* **1999**, *111*, 7727−7735.
(33) Rols, S.; Almairac, R.; Henrard, L.; Anglaret, E.; Sauvajol, J. E. *Eur. Phys. J. B* **1999**, *10*, 263−270.
(34) Bandow, S.; Asaka, S.; Saito, Y.; Rao, A. M.; Grigorian, L.; Richter, E.; Eklund, P. C. *Phys. Rev. Lett.* **1998**, *80*, 3779−3782.
(35) Rao, A. M.; Richter, E.; Bandow, S.; Chase, B.; Eklund, P. C.; Williams, K. A.; Fang, A.; Subbaswamy, K. R.; Menon, M.; Thess, A.; Smalley, R. E.; Dresselhaus, G.; Dresselhaus, M. S. *Science* **1997**, *275*, 187−191.
(36) Rinzler, A. G.; Liu, J.; Dai, H.; Nikolaev, P.; Huffman, C. B.; Rodrıguez-Macıas, F. J.; Boul, P. J.; Lu, A. H.; Heymann, D.; Colbert, D. T.; Lee, R. S.; Fischer, J. E.; Rao, A. M.; Eklund, P. C.; Smalley, R. E. *Appl. Phys. A* **1998**, *67*, 29−37.
(37) Wildoer, J. W. G.; Venema, L. C.; Rinzler, A. G.; Smalley, R. E.; Dekker, C. *Nature* **1998**, *391*, 59−62.
(38) Mawhinney, D. B.; Naumenko, V.; Kuznetsova, A.; Yates, J. T., Jr.; Liu, J.; Smalley, R. E. *Chem. Phys. Lett.* **2000**, *324*, 213−216.
(39) Kuznetsova, A.; Yates, J. T., Jr.; Simonyan, V. V.; Johnson, J. K.; Huffman, C. B.; Smalley, R. E. *J. Chem. Phys.* **2001**, *115*, 6691−6698.
(40) Simonyan, V. V.; Johnson, J. K. In preparation.
(41) Hershkowitz, F.; Madiara, P. D. *Ind. Eng. Chem. Res.* **1993**, *32*, 2969−2974.
(42) Siriwardane, R. V.; Shen, M. S.; Fisher, E. P.; Poston, J. A. *Energy Fuels* **2001**, *15*, 279−284.
(43) Allen, M. P.; Tildesley, D. J. *Computer Simulation of Liquids*; Clarendon: Oxford, 1987.
(44) Silvera, I. F.; Goldman, V. V. *J. Chem. Phys.* **1978**, *69*, 4209−4213.
(45) Wang, Q.; Johnson, J. K. *Fluid Phase Equilib.* **1997**, *132*, 93−116.
(46) Crowell, A. D.; Brown, J. S. *Surf. Sci.* **1982**, *123*, 296.
(47) Wang, Q.; Johnson, J. K. *Mol. Phys.* **1998**, *95*, 299−309.
(48) Monthioux, M.; Smith, B. W.; Burteaux, B.; Claye, A.; Fischer, J. E.; Luzzi, D. E. *Carbon* **2001**, *39*, 1251−1272.
(49) U.S. Patent 5,346,683, 1994.